(19) Europäisches Patentamt
European Patent Office
Office européen des brevets

(11) Publication number: **0 676 839 A1**

(12) **EUROPEAN PATENT APPLICATION**

(21) Application number: 95302112.8

(22) Date of filing: 29.03.95

(51) Int. Cl.^{6}: H01S 3/18, H01S 3/19

(30) Priority: 04.04.94 US 223341
09.01.95 US 371000

(43) Date of publication of application:
11.10.95 Bulletin 95/41

(84) Designated Contracting States:
DE FR GB

(71) Applicant: AT & T Corp.
32 Avenue of the Americas
New York, NY 10013-2412 (US)

(72) Inventor: Capasso, Federico
42 Westbrook Road
Westfield, New Jersey 07090 (US)
Inventor: Cho, Alfred Yi
11 Kenneth Court
Summit, New Jersey 07901 (US)
Inventor: Faist, Jerome
239 Country Club Lane
Scotch Plains, New Jersey 07076 (US)
Inventor: Hutchinson, Albert Lee
1359 River Road
Piscataway, New Jersey 08854 (US)
Inventor: Luryi, Serge
907 Papen Road
Bridgewater, New Jersey 08807 (US)
Inventor: Sirtori, Carlo
2 Hillside Avenue
Summit, New Jersey 07901 (US)
Inventor: Sivco, Deborah Lee
Plainfield Avenue
Warren, New Jersey 07059 (US)

(74) Representative: Watts, Christopher Malcolm Kelway, Dr.
AT&T (UK) Ltd.
5, Mornington Road
Woodford Green Essex, IG8 0TU (GB)

(54) **Unipolar semiconductor laser.**

(57) This application discloses, a unipolar laser. An exemplary embodiment of the laser was implemented in the GaInAs/AlInAs system and emits radiation of about 4.2μm wavelength. Embodiments in other material systems are possible, and the lasers can be readily designed to emit at a predetermined wavelength in a wide spectral region. We have designated the laser the "quantum cascade" (QC) laser. The QC laser comprises a multilayer semiconductor structure that comprises a multiplicity of essentially identical undoped "active" regions (11), a given active region being separated from an adjoining one by a doped "energy relaxation" region (12). The active region comprises one or more quantum wells. In one embodiment of the invention the active region is selected such that a radiative transition from a third to a second energy state substantially is a "diagonal" transition, and in another embodiment the active region is selected such that the radiative transition substantially is a "vertical" one. In the latter case the energy relaxation region advantageously comprises a superlattice Bragg reflector for charge carriers (typically electrons) of energy corresponding to the third energy state.

FIG. 1

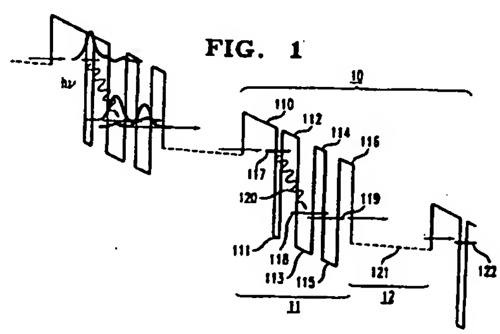

EP 0 676 839 A1

Jouve, 18, rue Saint-Denis, 75001 PARIS

Field of the Invention

This application pertains to the field of injection semiconductor lasers.

Background of the Invention

R. F. Kazarinov et al. (Soviet Physics-Semiconductors, Vol. 5(4), p. 707 (1971)) predicted the possibility of amplification of electromagnetic waves in a semiconductor superlattice structure. Since the publication of this seminal paper, the feasibility of a unipolar quantum well semiconductor laser has been considered by many workers in the field. See, for instance, S. J. Borenstain et al., Applied Physics Letters, Vol. 55(7), p. 654 (1989); Q. Hu et al., Applied Physics Letters, Vol. 59(23), p. 2923 (1991); A. Kastalsky et al., Applied Physics Letters, Vol. 59(21), p. 2636 (1991); and W. M. Yee et al., Applied Physics Letters, Vol. 63(8), p. 1089 (1993). However, to the best of our knowledge, the prior art does not disclose observation of lasing in any of the proposed unipolar structures.

Those skilled in the art are aware of the advantages potentially offered by some types of unipolar injection laser. Among these are a frequency response that is not limited by electron/hole recombination, a narrow emission line because the line-width enhancement factor is (theoretically) zero, and a weaker temperature dependence of the lasing threshold than in conventional (i.e., bipolar) semiconductor lasers. Furthermore, appropriately designed unipolar semiconductor lasers can have an emission wavelength in the spectral region from the mid-infrared (mid-IR) to the submillimeter region, exemplarily in the approximate range 3-100 μm, that is entirely determined by quantum confinement. The emission wavelength can be tailored using the same heterostructure material over the above mentioned wide spectral region, a portion of the spectrum not easily accessible with diode semiconductor lasers. Furthermore, unipolar lasers can use relatively wide bandgap, technologically mature materials (e.g., utilize GaAs- or InP-based heterostructures), without reliance on temperature sensitive and difficult to process small bandgap semiconductors such as PbSnTe. Such unipolar lasers could, for instance, be advantageously used for pollution monitoring, industrial process control and automotive applications.

Prior art proposals for unipolar quantum well semiconductor lasers typically involve use of resonant tunneling structures. For instance, W. M. Yee et al., (op. cit.) analyzed two coupled quantum well structures, each of which contains an emission quantum well sandwiched between energy filter wells, the coupled quantum well assembly sandwiched between n-doped injector/collector regions. The energy filter wells, respectively, have only one quasibound state (E_1 and E_3, respectively), and the emission quantum well has more than one quasibound state, with intersubband transitions taking place between two of the states ($E_2^{(2)}$ and $E_2^{(1)}$). When, by means of an applied electric field, E_1 becomes substantially aligned with $E_2^{(2)}$, electrons from the injector can resonantly populate $E_2^{(2)}$. If, at the same applied field, E_3 is substantially aligned with $E_2^{(1)}$ then the latter can be resonantly depleted into the collector. If the time constant for the former process is longer than the time constant for the latter then a population inversion in the emission quantum well could, at least in principle, be achieved.

As those skilled in the art will appreciate, the optical output power obtainable from a structure of the type analyzed by Yee et al., (i.e., a structure that comprises a single set of coupled quantum wells) is typically too small to be of practical interest. In principle this shortcoming can be remedied by provision of a structure that comprises a multiplicity of said sets. However, it is known that, for fundamental reasons, lasing typically cannot be achieved in such a structure. For instance, application of a voltage across such a multi-quantum well structure that comprises doped regions will typically result in a non-uniform field in the device, with attendant negative resistance and instability. See, for instance, K. K. Choi et al., Physical Review B, Vol. 35 (8), p. 4172 (1987).

In view of the considerable potential commercial and scientific value of a unipolar semiconductor laser, especially one that can be designed to emit in the mid-IR spectral region, such a laser would be of substantial interest. This application discloses such a laser, to be referred to as the quantum cascade (QC) laser.

Summary of the Invention

The invention is as defined by the claims. In a broad aspect this application discloses a unipolar semiconductor injection laser. More specifically, the instant invention is embodied in an article that comprises a unipolar semiconductor (typically III-V semiconductor) laser that comprises a multilayer semiconductor structure containing doped semiconductor material of only a first conductivity type (typically n-type), and means for applying a voltage (including a normal operating voltage) across said multilayer semiconductor structure.

Significantly, the multilayer structure comprises a multiplicity (e.g., ten or more) of essentially identical

(i.e., exhibiting at most only substantially unavoidable minor differences) "active" regions, a given one of said active regions being separated from an adjoining active region by an "energy relaxation" region. Each of said active regions comprises one or more quantum wells. Associated with said at least one quantum well are at least two (but preferably three or more) energy states, said at least two (or three) energy states to be referred to, respectively as third and second (or third, second and first) energy states. The third energy state is at a higher energy than the second energy state, which in turn is (under appropriate bias) at a higher energy than the first energy state. The third, second and first energy states will also be referred to as the n=3, 2 and 1 states, respectively. Associated with said first, second and third energy states are, respectively, first, second and third wavefunctions. A wavefunction is "associated" with an energy state in a well if the centroid of the modulus square of the wavefunction is located in the well.

In a first embodiment of the invention the transition from the n=3 to the n-2 state substantially is a "diagonal" transition. An important aspect of the first embodiment is provision of the active region such that there is provided reduced spatial overlap between said third and second wavefunctions in a given active region. By "reduced spatial overlap" we mean herein overlap that is less than the overlap between the wavefunctions of states $E_2^{(2)}$ and $E_2^{(1)}$ of QW2 of any of the two structures of FIG. 1 of W. M. Yee et al., Applied Physics Letters, Vol. 63(8), p. 1089. Techniques for computing the overlap between wavefunctions in quantum well structures are known to those skilled in the art and do not require exposition. See, for instance, G. Bastard, "Wave Mechanics Applied to Heterostructures", Les Editions de Physique, Paris 1990. See also D. F. Nelson et al., Physical Review B, Vol. 35 (14), p. 7770 (1987). At least some (desirably substantially all) of the charge carriers undergo a (diagonal) radiative transition from the third to the second energy state.

The energy relaxation regions are selected to provide substantial energy relaxation and randomization of motion of charge carriers of the given conductivity type in a given energy relaxation region when a normal operating voltage is applied. Differently stated, and with reference to FIG. 1, the energy relaxation layer 12 exemplarily is selected to facilitate relaxation of charge carriers from the energy of the n=1 energy state 119 to the energy of the n=3 energy state 122 of the next active region, such that the carriers can tunnel into the n=3 state 122 of the next active layer. Exemplarily, the relaxation region thickness is 1-2 λ_E, where λ_E is the energy mean free path of the carriers in the energy relaxation region. At least some of the charge carriers are introduced into the given energy relaxation region by tunneling from said first energy state through a barrier layer. Typically, the active regions are at most lightly doped (exemplarily less than about 2-3 x $10^{16}cm^{-3}$) and preferably undoped (not intentionally doped), and the graded gap regions are doped (desirably not greatly exceeding about 10^{17} cm^{-3}, to minimize free carrier absorption) to exhibit conductivity of the given type, typically n-type. The energy relaxation region can be continuously (analog) or stepwise graded, but in currently preferred embodiments is digitally graded.

In a second embodiment of the invention the transition from the n=3 to the n=2 state substantially is a "vertical" transition, as will be described in greater detail below. In the case of a vertical transition laser according to the invention the energy relaxation regions preferably are superlattice Bragg reflectors.

A further significant aspect of the layer structure of a laser according to the invention is the provision of optical confinement of the lasing mode. This is accomplished by appropriate selection of layer compositions to result in a waveguide core of higher effective refractive index than that of the cladding layers.

As will be described in more detail below, the reduced overlap between the third and second energy states in the first embodiment materially contributes to attainment of a relatively long lifetime (τ_{32}) of the charge carriers in the third energy state. (The carriers are provided to the third energy state by tunneling from a first adjoining energy relaxation region). The lasing-relevant transition is the photon-emitting transition from the third to the second energy state. Carriers typically are removed from the second energy state by tunneling or phonon scattering into the first energy state. Associated with the carriers in the second energy state is a lifetime τ_{21}, which must be less than τ_{32}, to achieve population inversion between energy levels 3 and 2. Lifetime τ_{32} can be made relatively large by, e.g., appropriate choice of the wavefunction overlap, and τ_{21} can be made relatively small by, e.g., provision of an appropriately thin (e.g., less than 10 or 5 nm) barrier between the quantum wells associated with said first and second energy states. Preferably the active region is formed such that, with a normal operating voltage applied, the energy difference ΔE_{21} between second and first energy states is about $h\,\nu_{op}$ or larger, where h is Planck's constant and ν_{op} is the relevant optical phonon frequency. The preferred layer structure is also designed to provide, under a normal operating voltage, for tunneling of the carriers from the well associated with the first energy state into a second adjoining graded gap region.

The provision of energy relaxation regions is a significant aspect of the described embodiment of the invention, since it inter alia makes possible lasing in the multi-period structure before the appearance of negative resistance, thereby overcoming a significant shortcoming of previously proposed unipolar laser structures. The provision of reduced overlap of the third and second wavefunctions makes possible attainment of larger values of τ_{32} than are typically attainable in prior art structures, and is another significant aspect of preferred em-

bodiments.

A still further significant aspect is the substantial absence of dopant from the active regions of the QC laser, facilitating narrowing of the luminescence spectrum, thereby increasing the peak gain. The absence of doping is to be compared with the structure disclosed by J. Faist et al., (Electronics Letters, Vol. 29 (25), p. 2230 (Dec. 1993)) wherein, in addition to the graded gap region, a portion of the active region is doped. The structure exhibited a broad luminescence peak and was not capable of lasing, due to the absence of wave-guiding layers and the doping of a portion of the active region.

Brief Description of the Drawings

FIG. 1 schematically depicts a portion of the conduction band diagram of an exemplary laser according to the invention;

FIG. 2 is a schematic representation of the dispersion of the n=1, 2 and 3 energy states, respectively;

FIG. 3 shows exemplary data on the emission spectrum of a laser according to the invention, for various drive currents;

FIG. 4 provides data on optical power vs. drive current for another exemplary laser according to the spectrum;

FIG. 5 shows a portion of the spectrum of FIG. 3 in high resolution;

FIG. 6 shows data on threshold current vs. laser temperature for a still further laser according to the invention, indicating a value of 112K for the laser parameter T_o; and

FIG. 7 shows refractive index profile and mode intensity of an exemplary QC laser;

FIGs. 8 and 9 schematically illustrate an exemplary superlattice energy relaxation region;

FIG. 10 schematically depicts an exemplary laser according to the invention;

FIG. 11 shows schematically a portion of the conduction band diagram of a further exemplary laser according to the invention;

FIG. 12 shows the calculated electron transmission spectrum of an exemplary superlattice Bragg reflector; and

FIGs. 13 and 14 show the optical power from a single facet of an exemplary laser according to the invention, as a function of injection current, and the emission spectrum of the exemplary laser, respectively.

Detailed Description of Some Preferred Embodiments

Among the difficulties that have to be overcome before a practical unipolar laser can be achieved is the following: In III-V semiconductor materials of current interest, the excited state (e.g., $E_2^{(2)}$ of FIG. 1 of Yee et al.) non-radiative lifetime (τ_{NR}) typically is quite small (exemplarily about 1ps), if the intersubband separation (e.g., $E_2^{(2)} - E_2^{(1)}$ of FIG. 1 of Yee et al.) corresponds to a wavelength less than about 40 μm. This is typically due to the possibility in these materials of non-radiative decay due to optical phonon emission, for $E_2^{(2)} - E_2^{(1)} \geqq 2h\nu_{op}$, the optical phonon energy (typically about 30 meV). For $E_2^{(2)} - E_2^{(1)} < h\nu_{op}$, τ_{NR} is much larger, typically a few hundred picoseconds, being limited primarily by acoustic phonon scattering. J. Faist et al., Applied Physics Letters, Vol. 64(7), p. 872, (Feb. 1994).

Those skilled in the art will appreciate that a unipolar laser requires design features that make it possible to increase the excited state lifetime to a value substantially greater than is associated with prior art structures, such that a significant population inversion can be attained for transition energies $\geqq h\,\nu_{op}$. Exemplarily this is achieved by means of spatial separation between the ground state and the first excited state, with the relevant quantum wells being asymmetric and strongly coupled.

FIG. 1 schematically depicts the conduction band diagram of a portion of the multilayer semiconductor structure of an exemplary diagonal transition unipolar laser according to the invention under positive bias conditions corresponding to an electric field of 10^5V/cm. The quantum wells exemplarily are $Ga_{0.47}In_{0.53}As$ (to be referred to as "GaInAs"), and the barriers are $Al_{0.48}In_{0.52}As$ ("AlInAs"). The depicted portion comprises one period 10 of a (multiperiod) multilayer semiconductor structure, with the two adjoining periods also indicated. Each period comprises an active region 11 and an energy relaxation region 12, the former being substantially undoped (typically not intentionally doped), and the latter being doped. The energy relaxation region exemplarily is a digitally graded gap region. However, other energy relaxation regions are possible.

Electrons are tunnel injected into active region 11 through barrier 110. The active region includes coupled asymmetric quantum wells 111 and 113, separated by barrier 112. Associated with wells 111 and 113 are third energy state 117 and second energy state 118, respectively. Wavy line 120 indicates the photon-assisted tunneling transition responsible for luminescence (and lasing) in the exemplary structure. Electrons in the second energy state tunnel through barrier 114 into quantum well 115, occupying therein first energy state 119. Fur-

thermore, electrons tunnel through barrier 116 from well 115 into energy relaxation region 12. One of the adjoining active regions shown in FIG. 1 depicts the modulus square of the wavefunction associated with the first, second and third energy states, respectively.

As can be seen from FIG. 1, the wavefunction of the n=3 state can extend into the neighboring quantum well (e.g., 113) and beyond, possibly resulting in some "leakage" of electrons out of the n=3 state. This occurs because the QC laser typically operates under a strong applied electric field. The main effect of the extension of the wavefunction into the continuum typically is a decrease of the injection efficiency, as electrons are escaping into the continuum instead of making a radiative transition. We believe that such escape can be reduced or prevented by appropriate choice of layer thicknesses, such that the layers form a Bragg reflector for the n=3 carriers (exemplarily electrons).

More specifically, it is possible to design, at least if the energy relaxation region is a digitally graded gap region, the energy relaxation region so as to behave as a Bragg mirror for the electrons at the energy of the n=3 level. Provision of an appropriately designed Bragg mirror can result in reflection of electrons back into the n=3 level, and thus prevent their escape into the continuum. Exemplarily, such Bragg reflection can be achieved if

$$l_{wJ}k_w + l_{bJ}k_b = \pi, \quad (1)$$

where $l_{w,J}$ and $l_{b,J}$ are the thicknesses, respectively, of the j-th well and barrier of the digitally graded region, and k_w and k_b the wave vector of the electron in the n=3 energy state.

For electrons having relatively low energy, the digitally graded region behaves as a medium with an effective conduction band edge difference ΔE_{eff}, measured with respect to the well (exemplarily GaInAs) conduction band edge, where

$$\Delta E_{effJ} = \Delta E_c[l_{bJ}/(l_{bJ} + l_{w,J})]. \quad (2)$$

In equation 2, ΔE_c is the conduction band discontinuity between the well and barrier materials. Selecting ΔE_{effJ} of the j-th well/barrier pair of the digitally graded region such that the conduction band edge of the region is substantially flat under the electric field designed for lasing (which is close to the value required for the "flat band" condition in the graded region), and using equations (1) and (2), one can ensure enhanced electron confinement in the n=3 state while allowing simultaneous transport through the digitally graded region of the electrons that did relax inside the active region.

Whereas a Bragg reflector is an optional feature of "diagonal transition" QC lasers, it is considered to be a preferred feature for "vertical transition" QC lasers. Vertical transition lasers will be discussed in more detail below.

Exemplarily, the active region 11 contains, going from higher to lower layer in the layer sequence, the following sequence of undoped layers: 4.5 nm barrier 110, 0.8 nm well 111, 3.5 nm barrier 112, 3.5 nm well 113, 3.0 nm barrier 114, 2.8 nm well 115, and 3.0 nm barrier 116.

For clarity's sake, FIG. 1 does not show the conduction band edge of digitally graded gap region 12, only the effective band edge 121 associated with the region. The graded gap region exemplarily consist of an AlInAs/GaInAs superlattice with constant period that is shorter than the electron thermal de Broglie wavelength (exemplarily of order 30 nm) in the material, and varying duty cycle to obtain a graded gap pseudoquaternary alloy. See, for instance, F. Capasso et al., Applied Physics Letters, Vol. 45(11), p. 1193 (1984). Exemplarily the graded gap region consists of the following n-doped (e.g., 1.5×10^{17} cm^{-3} Si) layer sequence, arranged to give an effective gap that varies from lower to higher values in going from left to right in FIG. 1: 1.8 nm well/1.2 nm barrier; 1.6/1.4 nm; 1.3/1.7 nm; 1.1/1.9 nm; 0.9/2.1 nm; 0.7/2.3 nm; 0.6 nm well.

As disclosed above, FIG. 1 pertains to the case of a QC laser with digitally graded gap energy relaxation region, and with an applied bias electric field of about 10^5 V/cm, sufficient to provide an electric field that approximately equals the opposing quasi-electric field associated with the conduction band grading, thus resulting in a substantially staircase-shaped conduction band edge. Those skilled in the art will appreciate that, in the absence of an applied bias, the band diagram of the structure has an overall sawtooth shape. See, for instance, Capasso et al., IEEE Transactions on Electron Devices, Vol. ED 30(4), p. 381 (1983).

We have carried out calculations which show that, at the depicted substantially "flat band" condition, graded gap energy relaxation regions 12 are quasi-neutral. Electrons relax in the energy relaxation regions and are injected by tunneling into the n = 3 excited state (the third energy state). The tunneling rate through trapezoidal barrier 110 is extremely high, exemplarily about $5ps^{-1}$, ensuring efficient filling of the n=3 level. The electronic states of the $Al_{0.48}In_{0.52}As/Ga_{0.47}In_{0.53}As$ coupled well structure of FIG. 1 were calculated in the envelope function approximation for various electric fields. The material parameters used are: ΔE_c (conduction band discontinuity) = 0.52eV, m^* (GaInAs) = 0.043 m_0, m^* (AlInAs) = 0.078 m_0, where m_0 is the free electron mass. For the nonparabolicity coefficient we used $\gamma = 1.13 \times 10^{-18}$ m^2. Nonparabolicities were taken into account using the method of D. F. Nelson et al. (op. cit.).

FIG. 2 is a schematic representation of the dispersion of the n=1, 2, 3 energy states parallel to the layers of the multilayer structure, with $k_\parallel$ being the corresponding wavevector component. The bottom of the subbands correspond to the first, second and third energy states. The subbands are nearly parallel, due to the small non-parabolicities of $k_\parallel$ not too far (typically $\leq$ 10 meV) from the bottom ($k_\parallel = 0$) and for not too large transition energies. As a result, electrons making radiative transitions to a lower subband (e.g., from n=3 to n=2) will all emit photons of essentially the same energy. The joint density of states of these transitions is therefore substantially delta function-like (in the absence of broadening). If a population inversion is created between the n=3 and n=2 states then the gain spectrum of the transition will be correspondingly narrow (collision limited), nearly symmetric, and typically much less sensitive to thermal broadening of the electron distribution than that associated with interband transitions in semiconductor diode lasers. Numeral 20 refers to the optical phonon-assisted transition from the n=3 level to the n=2 level. This process, in structures according to the invention, is between states of reduced wavefunction overlap and is accompanied by a large momentum transfer. Consequently, the relevant relaxation time (τ_{32}) can be relatively long, estimated about 4.3 ps at a bias of 10^5 V/cm in the above described embodiment. This can ensure population inversion between the n=3 and n=2 states, since the n=2 state empties into the n=1 state with a relaxation time estimated to be about 0.6 ps. This efficient relaxation is provided by quantum well 115. Strong inelastic relaxation via optical phonons with nearly zero momentum transfer occurs between strongly overlapped and closely spaced n=2 and n=1 subbands, as shown in FIG. 2. Finally, the tunneling escape time out of the n=1 state into the adjoining energy relaxation region typically is extremely short, exemplarily less than about 0.5 ps. This further facilitates population inversion.

The above described structure also facilitates injection into the excited state E_3 by reducing the tunneling escape probability into the continuum. The estimated escape time τ_{esc} is 6 ps, which leads to an injection efficiency $\eta_{in} = \tau_{esc}/(\tau_{esc} + \tau_{32}) \simeq 0.6$. The radiative efficiency of the n=3 to n=2 laser transition is estimated to be $\tau_{32}/\tau_R \approx 3\times10^{-4}$ at a field $\sim 10^5$ V/cm, where τ_R is the spontaneous emission lifetime, estimated to be about 13 ns. Calculations show that the product of $|z_{32}|^2\tau_{32}$ (where z_{32} = 1.5nm is the n=3 to n=2 transition matrix element) is weakly dependent on the electric field. The low or substantially zero doping level in the active region strongly reduces the linewidth of the n=3 to n=2 electroluminescence, as compared to more highly doped coupled wells, thus enhancing the peak material gain for the same radiative efficiency. Electric field tunable electroluminescence, up to room temperature, has recently been observed by us in similar AlInAs/GaInAs coupled-quantum-well heterostructures.

We have incorporated a multiplicity of the above described active region/energy relaxation region units into a waveguide structure. The resulting unipolar device lased at a wavelength of about 4.2μm. To the best of our knowledge, this is the first observation of laser action in a unipolar quantum well semiconductor structure.

Table 1 shows the layer sequence of an exemplary laser according to the invention. The 33.2 nm digitally graded region corresponds to below-defined "digital grating II", followed by below-defined "digital grating I", with the latter being above the former in the sequence of Table 1. The active region/digitally graded energy relaxation region sequence was repeated 25 times. Each unit of the sequence consisted of an undoped active region (3.0 nm barrier/2.8 nm well; 3.5 nm/3.5 nm; 3.5 nm 0.8 nm; 4.5 nm barrier) and one n-type (1.5 x 10^{17} cm^{-3}) "digital grating II". The 3.0 nm barrier corresponds to layer 110 of FIG. 1 and is, under a normal operating voltage, the most "upstream" layer of a given active region 11. The 14.6 nm digitally graded region corresponds to "digital grating I", and the 18.6 nm digitally graded region corresponds to "digital grating II". The compositions of the core and cladding regions were selected such that, at the lasing wavelength, the effective refractive index of the core region is larger than the effective indices of both the lower and upper cladding regions. The refractive index profile 70 of the layer structure is shown in FIG. 7, together with the calculated intensity profile 71 of the lasing mode. The confinement factor of the mode was calculated to be 0.496. A significant aspect of the waveguide structure that corresponds to the refractive index profile' of FIG. 7 is the presence of doped (10^{17} cm^{-3}) 300 nm GaInAs layers that correspond to refractive index regions 72 and 73, which sandwich the active region that corresponds to refractive index region 74 and which significantly enhance mode confinement by providing large refractive index steps. Those skilled in the art will appreciate that such enhancement layers are novel, being unsuitable for use in conventional diode lasers since they would introduce unacceptable loss due to interband absorption. The entire multilayer structure was grown epitaxially, by MBE, on a conventional n^+-doped InP wafer.

Table 1

		n-doping level (cm^{-3})	Thickness (nm)	
Contact layer	GaInAs Sn doped	2.0×10^{20}	20.0	
	GaInAs	1.0×10^{18}	670.0	
	AℓGaInAs Graded	1.0×10^{18}	30.0	
Waveguide cladding	AℓInAs	5.0×10^{17}	1500.0	
	AℓInAs	1.5×10^{17}	1000.0	
Waveguide core	AlGaInAs Digitally graded	1.5×10^{17}	18.6	
	Active region	undoped	21.1	
	GaInAs	1.0×10^{17}	300.0	
	AℓGaInAs Digitally graded	1.5×10^{17}	14.6	
	AlGaInAs Digitally graded	1.5×10^{17}	18.6	x 25
	Active region	undoped	21.1	
	GaInAs	1.0×10^{17}	300.0	
	AℓGaInAs Digitally graded	1.5×10^{17}	33.2	
Waveguide cladding	AℓInAs	1.5×10^{17}	500.0	
	Doped n^+InP substrate			

Table II

Digital Grating I	
AlInAs	1.2 nm
GaInAs	6.5 nm
AlInAs	1.2 nm
GaInAs	4.5 nm
AlInAs	1.2 nm

Table III

Digital Grating II	
GaInAs	1.8 nm
AlInAs	1.2 nm
GaInAs	1.6 nm
AlInAs	1.4 nm
GaInAs	1.3 nm
AlInAs	1.7 nm
GaInAs	1.1 nm
AlInAs	1.9 nm
GaInAs	0.9 nm
AlInAs	2.1 nm
GaInAs	0.7 nm
AlInAs	2.3 nm
GaInAs	0.6 nm

The thus produced multilayer wafer was conventionally lithographically processed into mesa etched ridge waveguides of width 12μm. The length of the waveguides (varying from 0.5 to 2.8 mm) was defined by cleaving. This also was conventional. The cleaved facets provided the reflection means that define the laser cavity. Facet reflectivity was about 0.27. Conventional ohmic contacts were provided to the top contact layer and to the substrate. An exemplary device, of length 500 μm, was soldered to a ceramic holder, mounted in a conventional flow dewar and tested by injection of 20 ns current pulses (10^{-3} duty cycle) and measurement of the emission spectrum by conventional means (Nicolet Fourier transform IR spectrometer).

FIG. 10 schematically depicts the above described exemplary laser according to the invention. Numerals 101-104 refer to the substrate, 500 nm AlInAs layer, 33.2 nm digitally graded layer, and 300 nm GaInAs layer, respectively. The digitally graded layer 103 consists of digital grating I above digital grating II. Numerals 105 and 106 refer to the active region and the 18.6 nm digitally graded layer (digital grating II), respectively. Layers 105 and 106 are repeated several (e.g., 25) times. Numerals 107-110 refer to the 14.6 nm digitally graded (digital grating I) layer, the second 300 nm GaInAs layer, the further 21.1 nm active region, and the further 18.6 nm digitally graded (digital grating II) layer, respectively. Numerals 111-115 refer to the 1000 nm cladding layer, the 1500 nm cladding layer, the 30 nm graded contact layer, the 670 nm GaInAs contact layer, and the 20 nm highly doped (2×10^{20} cm^{-3}) GaInAs contact layer, respectively. Numerals 116and 117refer to conventional metal contact layers. Those skilled in the art will appreciate that FIG. 10 is schematical, with some conventional features (e.g., re-growth) not shown, and that layer thicknesses and other dimensions are not drawn to scale or in proportion.

FIG. 3 shows exemplary results at 10 K. Above a device current of about 850 mA, corresponding to a threshold current density of about 15 kA/cm², the signal amplitude increases abruptly by orders of magnitude, accompanied by dramatic line-narrowing. This is direct manifestation of laser action. In other QC lasers we have observed lasing at liquid nitrogen temperature, with powers approaching 20 mW for a 1.2 mm long cavity under pulsed operation. Lasing temperatures as high as 125K have been attained. Design and packaging optimization is expected to result in QC lasers capable of CW operation at even higher temperatures.

FIG. 4 shows optical power vs. device current at 10K for a laser substantially as described, but of length 720 μm. The threshold current density is 11 kA/cm², corresponding to 8.7 V across the device, with peak optical power from a single facet of about 8.5 mW. This power was limited by the collection efficiency (40%) of the apparatus and by the divergence of the beam (±40°) normal to the layers. FIG. 5 shows a portion of the spectrum at higher resolution. Well defined, nearly equally spaced ($\Delta\nu = 2.175$ cm^{-1}) longitudinal modes were observed. The linewidth of the dominant mode was about 0.3 cm^{-1}, presently limited by heating effects and mode hopping during the pulse. Theory predicts, for single longitudinal mode continuous wave (cw) operation, a

Schawlow-Townes linewidth with negligible linewidth enhancement factor, compared to conventional semiconductor lasers.

The laser wavelength essentially does not shift in the current range of FIG. 4, indicating that the electron density in the n=3 state is locked at the threshold value. Using measured results and estimated values of τ_{32} and τ_{esc} (τ_{esc} is the escape time from the n=3 state into the continuum), we estimate a population inversion n_s = 1.7 x 10^{11} cm^{-2}, comparable to the electron density in the graded gap region.

In other experiments, we obtained from a 1.2 mm long laser an output power of 30 mW at 10K and 4 mW at 125K, and from a 2.8 mm long laser a power of 130 mW at 10K.

FIG. 6 shows data on the temperature dependence of the threshold current of a 1.2 mm QC laser. The data shows that the conventional laser parameter T_o had the value 112K, indicative of desirably low temperature dependence of the threshold. The observed lasing mode was polarized normal to the layers of the multilayer structure, due to the selection rule for intersubband transitions.

Digital grading of the energy relaxation regions is not required, and conventional (continuous or discontinuous) "analog" grading is contemplated. Indeed, the energy relaxation region need not be a graded gap region, and all other means for attaining carrier energy relaxation in the region between adjacent active regions are contemplated. Exemplary of such other means are a doped, relatively thick, uniform quantum well, and a superlattice region.

The former exemplarily is doped to a level of order $10^{17}/cm^3$, and has a thickness (e.g., 1-2 λ_E) selected to result in energy relaxation of the carriers to the bottom of the band in the region. Desirably, the composition of the quantum well (e.g., $Al_xGa_{1-x}As$) is selected such that, under the bias required for lasing, the conduction band edge in the well is essentially lined up with the n=3 energy state of the adjacent (downstream) active region.

FIGS. 8 and 9 illustrate the design of an exemplary superlattice energy relaxation region, with the former showing the relevant aspects of the band structure under zero bias and the latter showing the aspects under lasing bias. Active region 11 is essentially the same as the active region of FIG. 1, and numeral 81 designates the superlattice energy relaxation region, with numerals 82-85 designating energy states. The quantum wells of the superlattice are selected such that, upon application of the lasing bias, energy states 82-85 become substantially aligned, forming miniband 90, with the miniband desirably positioned such that carriers from first energy state 119 can readily enter the miniband, and carriers can readily enter third energy state 117 of the adjacent (downstream) active region.

Still furthermore, the unipolar laser need not be n-doped but can, at least in principle, be p-doped, with the carriers preferably being the light holes to facilitate tunneling in appropriately strained layer semiconductors such as $In_xGa_{1-x}As$.

QC lasers can be implemented by conventional techniques (exemplary comprising MBE) in a variety of semiconductor systems. Exemplarily of such systems are AlGaAs/InAs, InP/GaInAs, and AlInAs/GaInAs, where the first member of a pair is the barrier material, and the second member is the well material.

Quantum well structures similar to those described above (but differing therefrom inter alia with respect to doping of the active region, and lacking a waveguide structure) were recently described in the literature. J. Faist et al., Electronics Letters, Vol. 29 (25), p. 2230 (Dec. 1993), and J. Faist et al., Applied Physics Letters, Vol. 64, p. 1144, (1994). These papers disclose observation of luminescence, but do not report observation of lasing. Indeed, the structures disclosed in these papers were not designed, and were unsuitable, for laser action.

Unipolar lasers have the unique property that carriers in the active region form a unipolar plasma. We have discovered that the spatial position of such a plasma can be controlled by means of an appropriate electric field, to be designated the "control" field. The ability to control the spatial position of the plasma in the laser structure makes possible, for instance, controlled steering of the laser output beam, and external control of the modal gain of the laser, i.e., control of the overlap of the optical wave cross section with the spatial profile of the gain.

In general, the electric control field will be applied such that at least a component of the control field lies in the plane of the layer structure (that is to say, in a plane normal to the direction of current flow in the layer structure). For instance, the control field can be applied in the direction perpendicular to the axis of the laser cavity by one or more sets of parallel planar conductors, possibly but not necessarily, integrated with the laser structure. Exemplarily, the planar conductors are metallic layers deposited over the sidewall dielectric.

Another contemplated approach to the application of the control field utilizes the piezo-electric property of the laser material, especially if the QC laser is implemented in III-V heterostructure materials. For instance, generation of an acoustic wave (either as a traveling or a standing wave) can result in a spatially varying electric field in the material, and thus can result in an acoustoelectric interaction between the acoustic wave and the carriers. For instance, an acoustic wave, propagating in the direction parallel to the axis of the laser cavity,

can establish a periodic structure in the density of carriers (which, in turn, leads to periodic spatial structure in the optical gain and the refractive index) which can, for instance, serve as a "grating" for distributed feedback. This effect, for instance, makes it possible to vary the frequency of the lasing mode by varying the frequency of the acoustic wave.

Those skilled in the art will appreciate that the piezo-electrically generated control field need not be due to an acoustic wave but can be generated by other means, e.g., by application of static or time-varying stress.

As was mentioned above, the invention can be embodied in a laser in which the n = 3 and n = 2 states have strong spatial overlap, such that the 3→2 transition primarily takes place in a given quantum well. Such a laser has a "vertical" transition, whereas a laser that has the n = 3 and n = 2 states primarily associated with different quantum wells can be said to primarily have "diagonal" transitions. For instance, FIG. 11 shows that the wavefunctions of both the n=3 and n=2 states extend into quantum well 1114, but that the overlap of the wavefunctions is greatest in well 1113. As a consequence, the 3→2 transition will primarily be a vertical one.

M. Helm et al., Physical Review Letters, Vol. 63, p. 74 (1989) have reported far infrared electroluminescence ($\lambda \sim 100\mu m$) associated with vertical intersubband transitions in a multiquantum well structure through sequential resonant tunneling. Lasers with primarily vertical transition will now be discussed in more detail.

We have found that vertical transition lasers according to the invention can, under appropriate circumstances, have advantages over diagonal transition lasers according to the invention. For instance, being typically less sensitive to unavoidable interface roughness and impurity fluctuations, the former can have a narrower gain spectrum (and thus a lower threshold) than the latter. Of course, those skilled in the art will understand that vertical transition lasers will generally not have reduced spatial overlap between the third and second wavefunctions in a given active region. The absence of such reduced overlap will generally result in somewhat reduced lifetime τ_{32}. However, we have found that the carrier residence time in the n=2 level can, through appropriate design of the active region and/or the energy relaxation region, be made sufficiently short such that a population inversion can be readily obtained.

FIG. 11 schematically depicts the conduction band diagram of a portion of the multilayer semiconductor structure of an exemplary "vertical transition" unipolar laser according to the invention under positive bias conditions corresponding to an electric field of 8.5×10^4 V/cm. The conventions are the same as in FIG. 1, except that "minibands" 1121 and 1123, and "minigap" 1122 are shown. The minibands and minigap are associated with superlattice Bragg reflector 1112, and indicate energy regions in which the superlattice is, respectively, relatively transparent and relatively opaque to electrons. Numeral 1111 refers to an active region, numerals 1112' and 1111' refer to the upstream Bragg reflector and active region, respectively, and 1111" refers to the downstream active region. Third and second energy levels 1117 and 1118 are primarily associated with quantum well 1113, and first energy state 1119 is primarily associated with quantum well 1114. Wavy arrow 1120 indicates the (photon-emitting) vertical transition from the third to the second level. Dashed line 1124 indicates the effective conduction band edge of superlattice Bragg reflector 1112', with electrons injected into the active region by tunneling through barrier layer 1115.

It will be appreciated that a superlattice Bragg reflector of the type described herein is a reflector for electrons in the n=3 state but provides energy relaxation for low energy electrons, e.g., the electrons in the n=1 state.

In an exemplary vertical transition laser according to the invention each one of 25 active regions consisted of a 6.5 nm AlInAs barrier layer through which electrons are tunnel injected into the upper energy level of a 4.5 nm InGaAs well coupled to a 3.6 nm InGaAs well by a 2.8 nm AlInAs barrier. The active regions were left undoped, and the seven center layers of each superlattice Bragg reflector were doped with Si ($n = 3 \times 10^{17}$ cm^{-3}), yielding a sheet density per period of 4×10^{11} cm^{-2}. The lifetime τ_{32} was calculated to be 1.8 ps. This allowed population inversion since electrons in the second energy level relax to the first level through optical phonon emission, with near zero momentum transfer, in a time τ_{21} = 0.6 ps. Electrons escape out of the first energy state through a 3.0 nm AlInAs barrier into the lower miniband of the downstream Bragg reflector.

The superlattice Bragg reflectors were designed such that the effective conduction band edge was substantially flat under the applied field, as described above, and such that each well and barrier pair accommodates a half electron DeBroglie wavelength, thus satisfying the Bragg condition. The barrier length l_b and well length l_w will however depart individually from a quarter wavelength. In mathematical terms, we require that the effective conduction band potential $V(x_j)$ of the graded gap at the position x_j of the j^{th} period, be approximated by

$$V(x_j) \cong \Delta E_c \frac{l_{b_j}}{l_{w_j} + l_{b_j}} \quad (3)$$

where ΔE_c is the conduction band discontinuity between the barrier and well material (=0.52 eV). This results in a quasi electric-field which cancels the applied field at threshold F_{th}:

$$V(x_j) - V(x_{j-1}) = -F_{th}(l_{bj} + l_{wj}) \quad (4)$$

We have also for each layer pair l_{wj}, l_{bj} the Bragg reflection condition of equation (1) above, namely,

$$k_{wj}l_{wj} + k_{bj}l_{bj} = \pi \quad (5)$$

where k_{wj} and k_{bj} are the wave numbers in the well and barrier materials. This condition ensures the constructive interference of the electronic waves reflected by all the periods. This set of equations is solved iteratively for each consecutive layer pair l_b and l_w of the graded gap superlattice. This procedure yields successive values of l_w = 2.1,2.1,1.6, 1.7, 1.3, and 1.0 nm and l_b =2.1,1.9,2.0,2.3,2.7 nm, right-to-left in FIG. 11.

Those skilled in the art will appreciate that the above described approach yields a region that has, under the appropriate bias, an electronic spectrum similar to the one of a regular superlattice, with a miniband facing the lower states of the active region for efficient carrier escape from the ground state of the lasing transition, and a minigap facing the upper state for efficient carrier confinement. This confinement is clearly apparent in FIG. 12, which shows the calculated transmission of the graded gap versus electron energy at the field F_{th} = 8.5 x 10^4 V/cm, corresponding to the laser threshold. The transmission is very small (~ 10^{-4}) at the energy E_3 corresponding to the upper state n=3, while remaining sufficiently large (> 10^{-1}) at the energy E_1 to insure a short escape time (≥0.6ps) from the n=1 state into the superlattice.

An exemplary vertical transition unipolar laser according to the invention had the layer structure shown in Table IV, with further details provided by Tables V-VIII.

Table IV

			n-doping level	Thickness (nm)	
↑ Contact	GaInAs		1×10^{20} cm^{-3}	10	
↓	$Ga_{0.5(1-x)}Al_{0.5x}InAs$	x=1 → 0 (top)	7×10^{18} cm^{-3}	30	
↑ Waveguide cladding	AℓInAs		7×10^{18} cm^{-3}	700	
	AℓInAs		4×10^{17} cm^{-3}	600	
↓	AℓInAs		1.5×10^{17} cm^{-3}	1000	
↑	$Ga_{0.5(1-x)}Al_{0.5x}InAs$	x=0 → (top)	2×10^{17} cm^{-3}	30	
	GaInAs		1×10^{17} cm^{-3}	300	
Waveguide core	$Ga_{0.5x}Al_{0.5(1-x)}InAs$	Digital grating I′	2×10^{17} cm^{-3}	14.6	
	$Ga_{0.5x}Al_{0.5(1-x)}InAs$	Digital grating II′	3×10^{17} cm^{-3}	25	↑ 25x
	Active region		undoped	19.9	↓
	$Ga_{0.5x}Al_{0.5(1-x)}InAs$	Digital grating III′	3×10^{17} cm^{-3}	12.4	
	GaInAs		1×10^{17} cm^{-3}	300	
	$Ga_{0.5x}Al_{0.5(1-x)}InAs$	Digital grating I′	2×10^{17} cm^{-3}	14.6	
↓	$Ga_{0.5x}Al_{0.5(1-x)}InAs$	Digital grating II′	2×10^{17} cm^{-3}	25	
↑ Waveguide cladding	AℓInAs		4×10^{17} cm^{-3}	20	
	AℓInAs		1.5×10^{17} cm^{-3}	500	
	Doped n InP substrate				

Table V

Digital Grating I'	
AℓInAs	1.2 nm
GaInAs	6.5 nm
AℓInAs	1.2 nm
GaInAs	4.5 nm
AℓInAs	1.2 nm

Table VI

Digital Grating II'		
doping level		
i	GaInAs	2.1 nm
i	AℓInAs	2.1 nm
i	GaInAs	2.1 nm
i	AℓInAs	2.1 nm
n	GaInAs	2.1 nm
n	AℓInAs	1.9 nm
n	GaInAs	1.6 nm
n	AℓInAs	2.0 nm
n	GaInAs	1.7 nm
n	AℓInAs	2.3 nm
n	GaInAs	1.3 nm
i	AℓInAs	2.7 nm
i	GaInAs	1.0 nm

Table VII

Digital Grating III'		
doping level		
i	GaInAs	2.1 nm
i	AℓInAs	2.1 nm
i	GaInAs	2.1 nm
i	AℓInAs	2.1 nm
n	GaInAs	2.1 nm
n	AℓInAs	1.9 nm

Table VIII

Active Region		
undoped	AlInAs	6.2 nm
undoped	GaInAs	4.5 nm
undoped	AlInAs	2.8 nm
undoped	GaInAs	3.6 nm
undoped	AlInAs	2.7 nm

The layer structure was processed into mesa etched ridge waveguides of width 14μm by conventional wet chemical etching. A 250 nm thick SiO_2 layer was then grown by chemical vapor deposition to provide insulation between the contact pads and the doped InP substrate. Windows were etched through the SiO_2 by plasma etching in CF_4 gas, exposing the top of the mesas. Non alloyed Ti/Au Ohmic contacts were provided to the top layer and the substrate. The processing was conventional. After processing, the samples were cleaved into 2.4-3mm long bars and soldered with In to a ceramic holder, wire bonded, and mounted in a He flow cryostat. Current pulses of 30ns duration were then injected in the device with a 20kHz repetition rate.

FIG. 13 shows peak optical power vs. drive current for a laser as described above. The structure had l_w = 2.1, 2.1, 2.1, 1.6, 1.7, 1.3 and 1.0 nm, and l_b = 2.1, 2.1, 1.9, 2.0, 2.3 and 2.7 nm. The transmissivity of this structure was substantially as shown in FIG. 12, but the separation between the n=2 state and the quasi-Fermi level in the graded superlattice was increased from ~ 50 meV to ~ 80 meV, resulting in a substantial decrease of thermally activated backfilling of electrons from the superlattice region into the n=2 state, and consequent improved laser characteristics.

The exemplary laser emitted radiation of wavelength 4.6μm, as shown by FIG. 14. The laser had a slope efficiency of 300 mW/A at 100K.

In currently preferred embodiments the energy difference $\Delta = E_2 - E_{Fn}$ is larger than the energy of the relevant optical phonons (preferably several times that phonon energy, e.g., ≥ 70 meV), in order to substantially avoid backfilling of electrons from the superlattice region into the n=2 state. In the above expression for Δ, E_2 is the energy of the n=2 level, and E_{Fn} is the quasi-Fermi energy in the lower miniband of the superlattice Bragg reflector region. Increased Δ typically results in improved high temperature performance of the laser, as exemplified by the marked improvement of a laser that had Δ ~ 80 meV, as compared to a very similar laser that had Δ ~ 50 meV. Exemplary data for the Δ ~ 80 meV laser are shown in FIGs. 13 and 14.

We currently believe that a laser according to the invention that primarily relies on vertical transitions is most advantageously implemented with superlattice Bragg reflectors as described above, but we also believe that such lasers can be implemented with other energy relaxation regions, although laser characteristics of the latter designs are expected to be inferior to those of the former. Furthermore, we currently believe that a laser according to the invention advantageously is based on a three-level (or possibly higher level) electron decay scheme as described above, but also believe that lasers based on a 2-level decay scheme (i.e., involving primarily the vertical n=3 to n=2 transition) are feasible. Such lasers will typically comprise superlattice Bragg reflectors that are highly reflective for n=3 electrons and highly transmissive for n=2 electrons under the normal operating bias.

Those skilled in the art will appreciate that the disclosed novel laser design principles can be embodied in a variety of laser structures, including structures that are not specifically discussed herein.

Claims

1. An article comprising a unipolar semiconductor laser, said laser comprising

   a) a multilayer semiconductor structure that comprises doped semiconductor material of only a first conductivity type; and

   b) means for applying a voltage across said multilayer semiconductor structure;

   CHARACTERIZED IN THAT

   c) said multilayer structure comprises a multiplicity of essentially identical active regions (e.g., 11), a given of said active regions being separated from an adjoining active region by an energy relaxation region (e.g., 12);

d) said active region comprises one or more quantum wells, associated with said quantum well or wells (e.g., 111, 113) being at least second and third energy states for charge carriers of the first conductivity type, with said third energy state (e.g., 117) being higher than said second energy state (e.g., 118);
e) said energy relaxation region is selected to provide for substantial energy relaxation of charge carriers of the first conductivity type in the energy relaxation region when a normal operating voltage is applied, at least some of said charge carriers being introduced into the energy relaxation region from said active region; and
f) at least some of the charge carriers of the first conductivity type undergo a radiative transition from the third to the second energy state.

2. Article according to claim 1, wherein said active region comprises two or more coupled quantum wells, associated with said coupled quantum wells are at least first, second and third energy states for said charge carriers, with the first energy state being lower than the second energy state when said normal operating voltage is applied; at least some of said charge carriers undergo a transition from the second to the first energy state and are introduced into the energy relaxation region from the first energy state.

3. Article according to claim 2, wherein the active region is substantially undoped, and the energy relaxation region comprises doped semiconductor material.

4. Article according to claim 2, wherein associated with the third and second energy states are third and second wavefunctions, and said active region is selected to provide reduced spatial overlap between said third and second wavefunctions.

5. Article according to claim 4, wherein the third, second and first energy states (117, 118, 119) are associated with third, second and first quantum wells (111, 113, 115), respectively, with an energy barrier (114) between said first and second quantum wells, and another energy barrier (112) between said second and third quantum wells, and said radiative transition from the third to the second energy level is substantially a diagonal transition.

6. Article according to claim 5, wherein said energy relaxation region comprises a doped continuously graded or stepwise graded gap region, or said energy relaxation region comprises a multiplicity of quantum wells.

7. Article according to claim 2, wherein said active region is selected such that said radiative transition from the third to the second energy state substantially is a vertical transition.

8. Article according to claim 7, wherein said energy relaxation region comprises a doped superlattice region that comprises a multiplicity of quantum wells, the superlattice region selected to provide a Bragg reflector for charge carriers of the first conductivity type having an energy that corresponds to the third energy state.

9. Article according to claim 1, wherein said multilayer semiconductor structure is selected to provide a waveguide for photons of energy corresponding to said radiative transition from the third to the second energy state.

10. Article according to claim 9, wherein said waveguide comprises a core that comprises said active region, and further comprises a doped semiconductor region having a refractive index that is higher than the refractive index of said active region.

FIG. 1

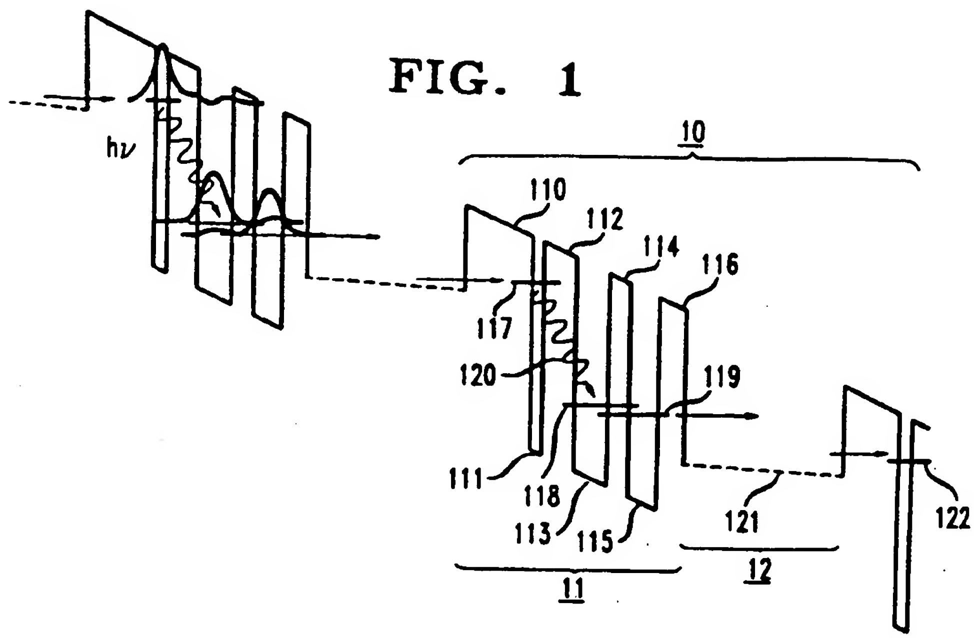

FIG. 2

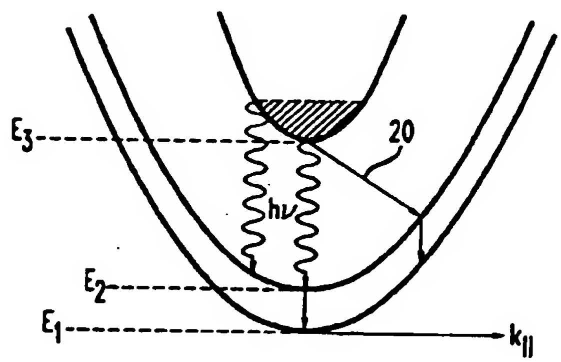

FIG. 6

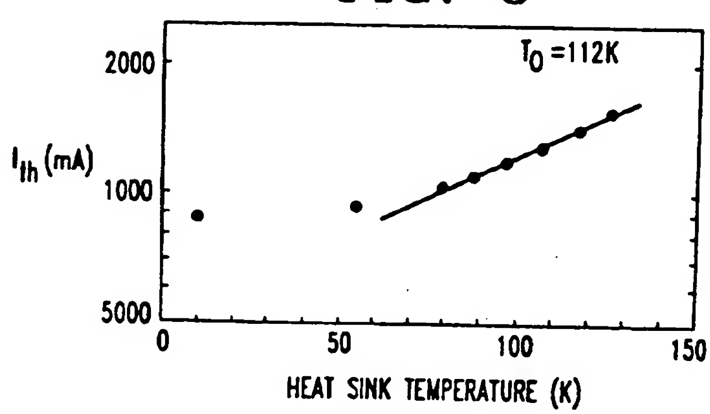

FIG. 3

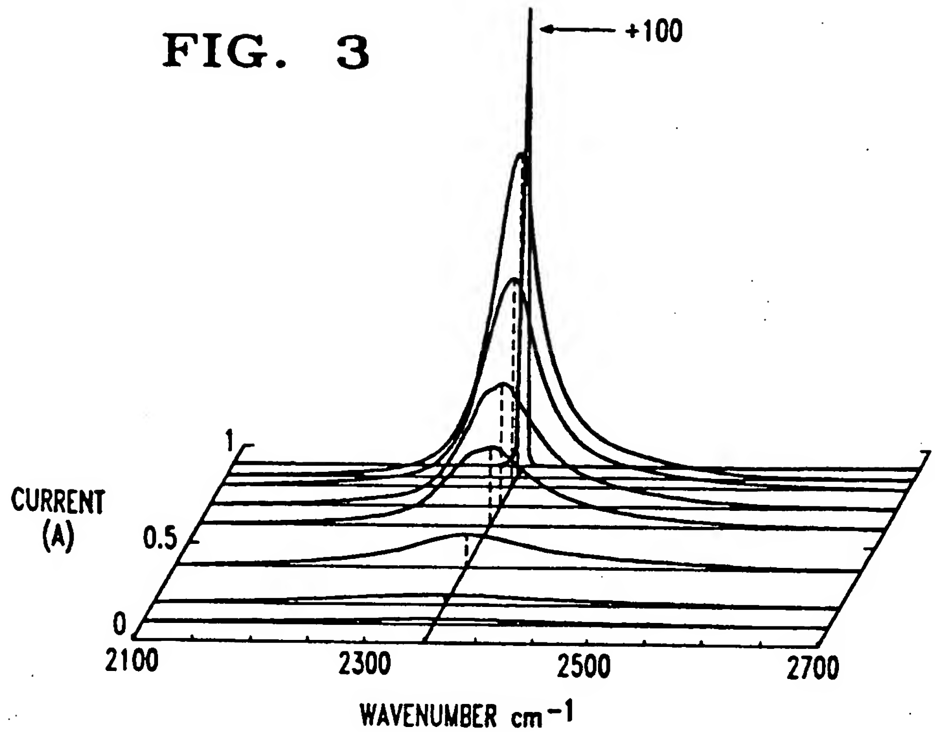
+100
CURRENT (A)
1
0.5
0
2100
2300
2500
2700
WAVENUMBER cm^-1

FIG. 4

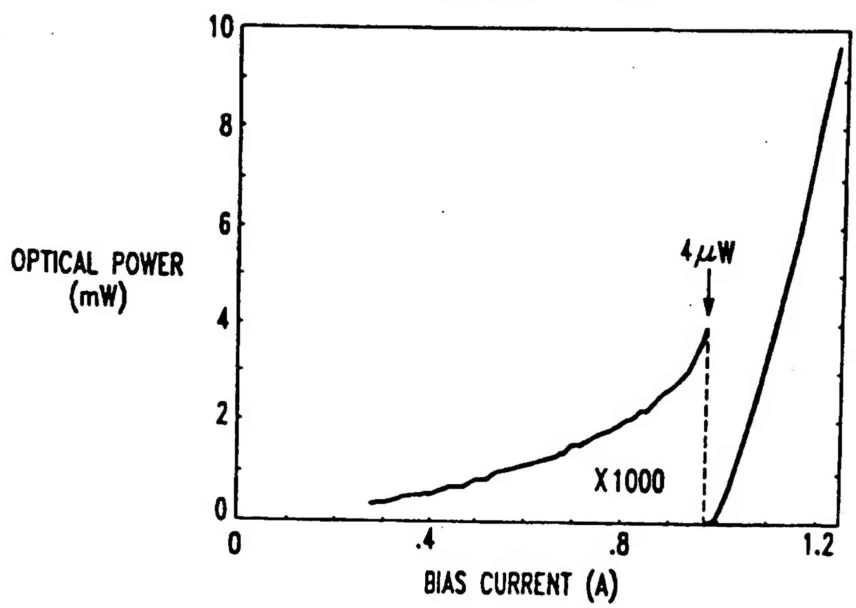
10
8
6
4
2
0
OPTICAL POWER (mW)
4μW
X1000
0
.4
.8
1.2
BIAS CURRENT (A)

FIG. 5

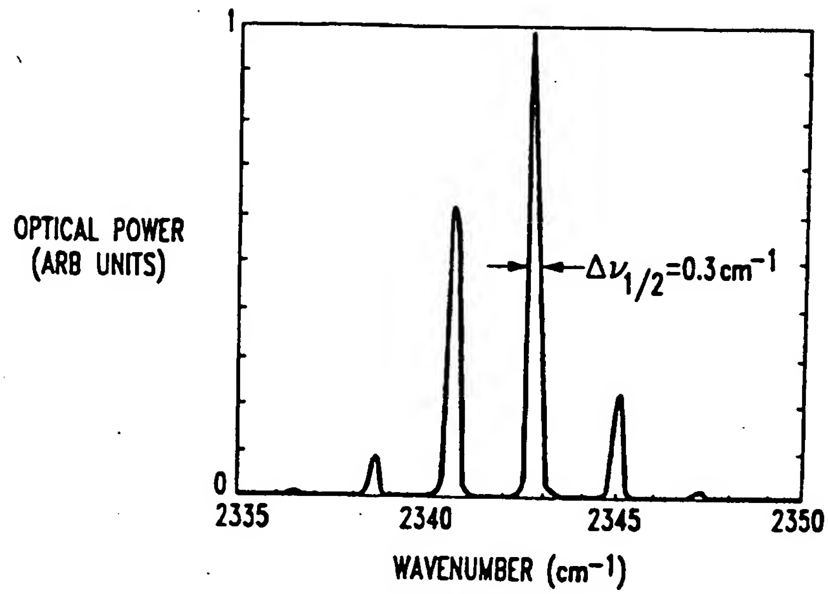
OPTICAL POWER
(ARB UNITS)
1
0
2335
2340
2345
2350
$\Delta\nu_{1/2}$=0.3cm^{-1}
WAVENUMBER (cm^{-1})

FIG. 7

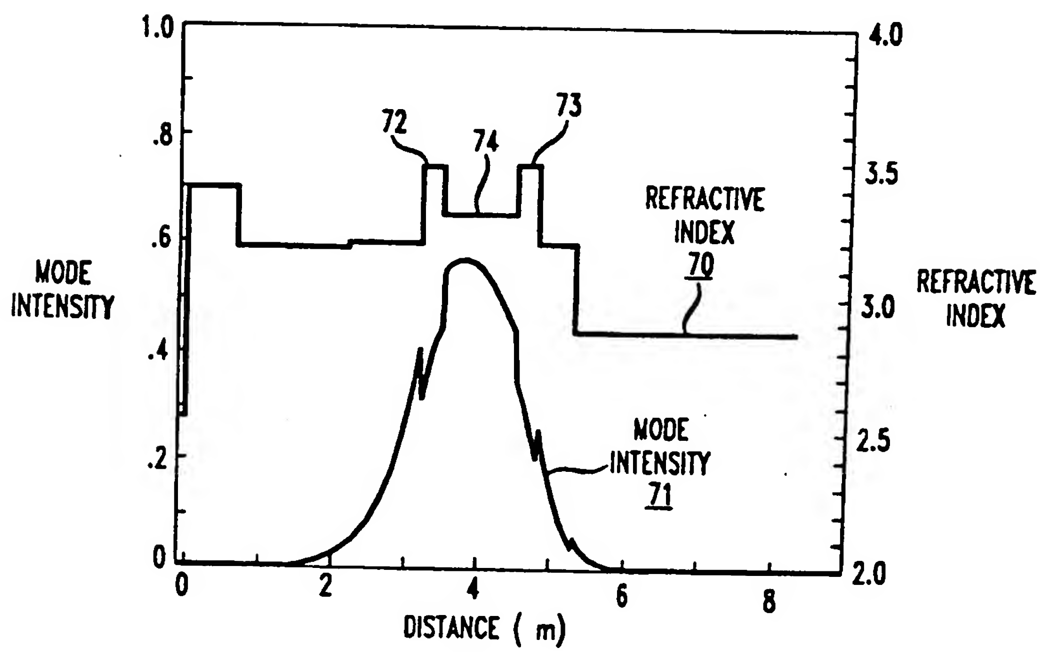
MODE
INTENSITY
1.0
.8
.6
.4
.2
0
72
74
73
REFRACTIVE
INDEX
70
MODE
INTENSITY
71
REFRACTIVE
INDEX
4.0
3.5
3.0
2.5
2.0
0
2
4
6
8
DISTANCE (m)

FIG. 8

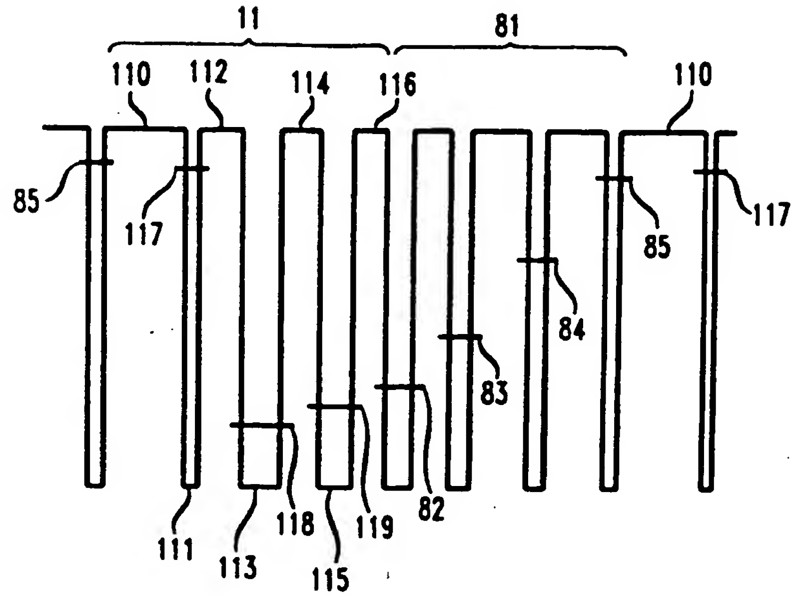
11
81
110
112
114
116
110
85
117
85
117
84
83
82
118
119
111
113
115

FIG. 9

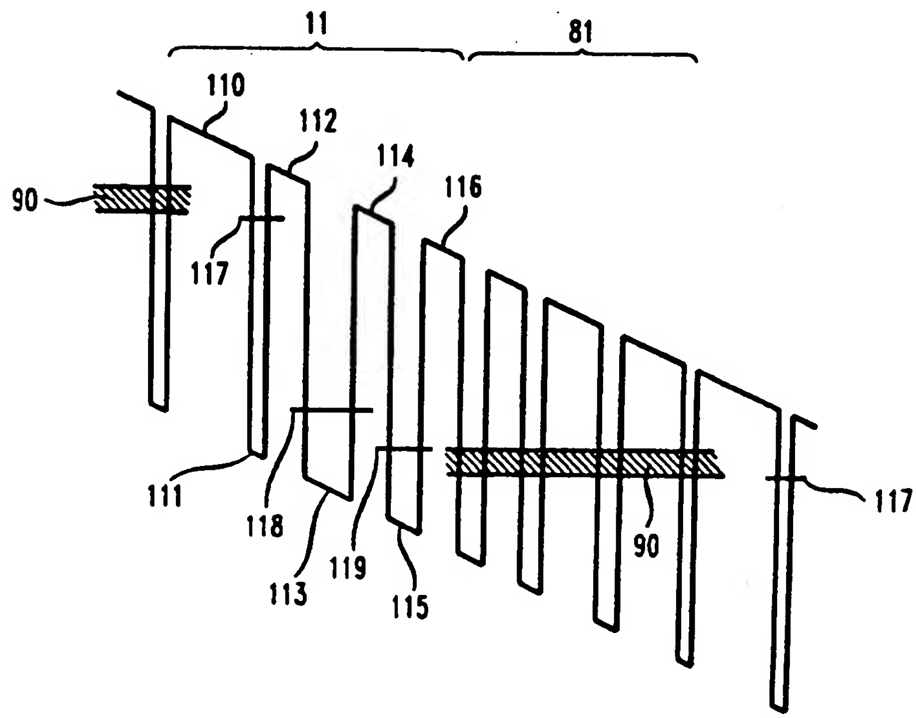
11
81
110
112
114
116
90
117
111
118
113
119
115
90
117

FIG. 10

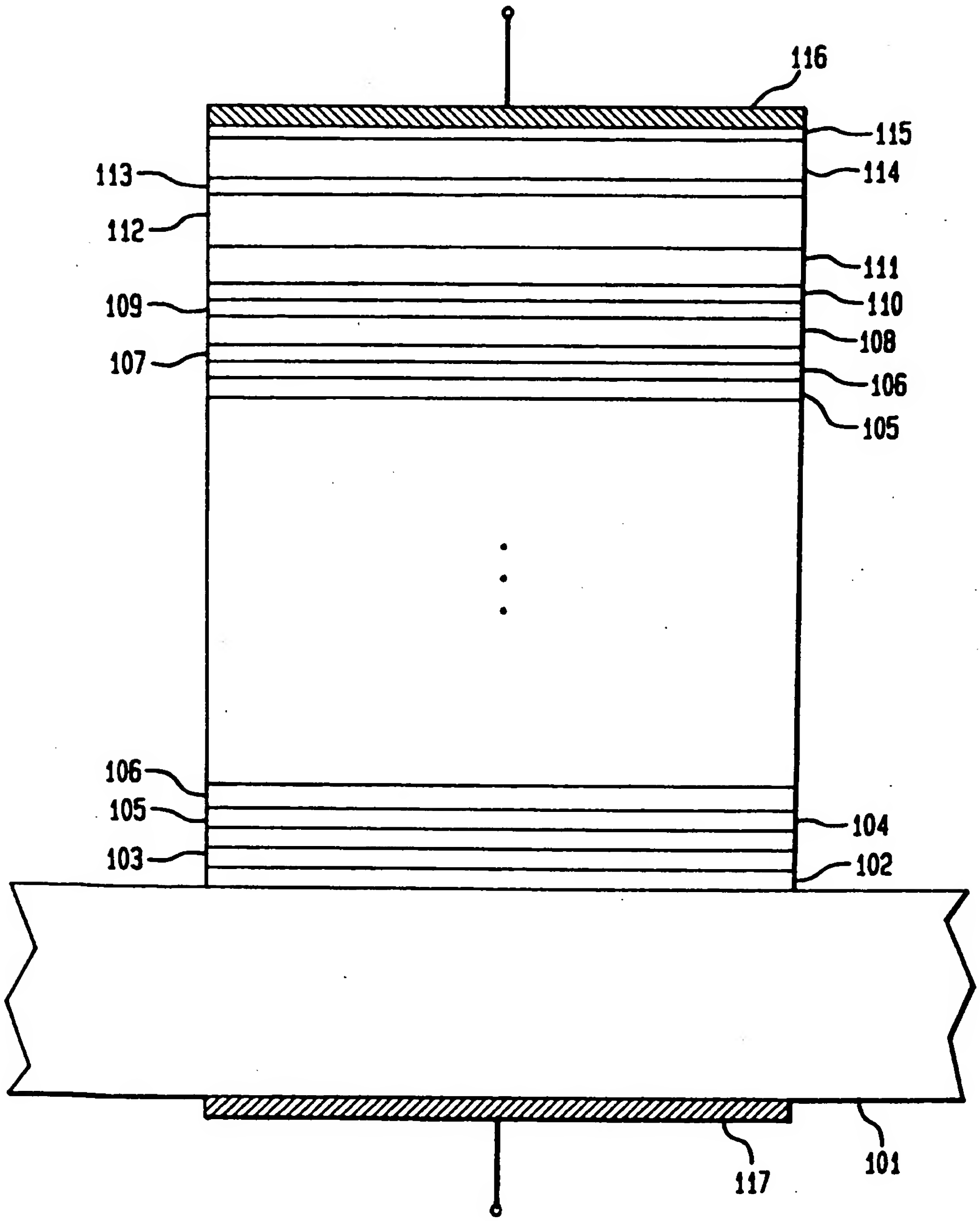
116
115
113
114
112
111
109
110
108
107
106
105
106
105
104
103
102
117
101

FIG. 11

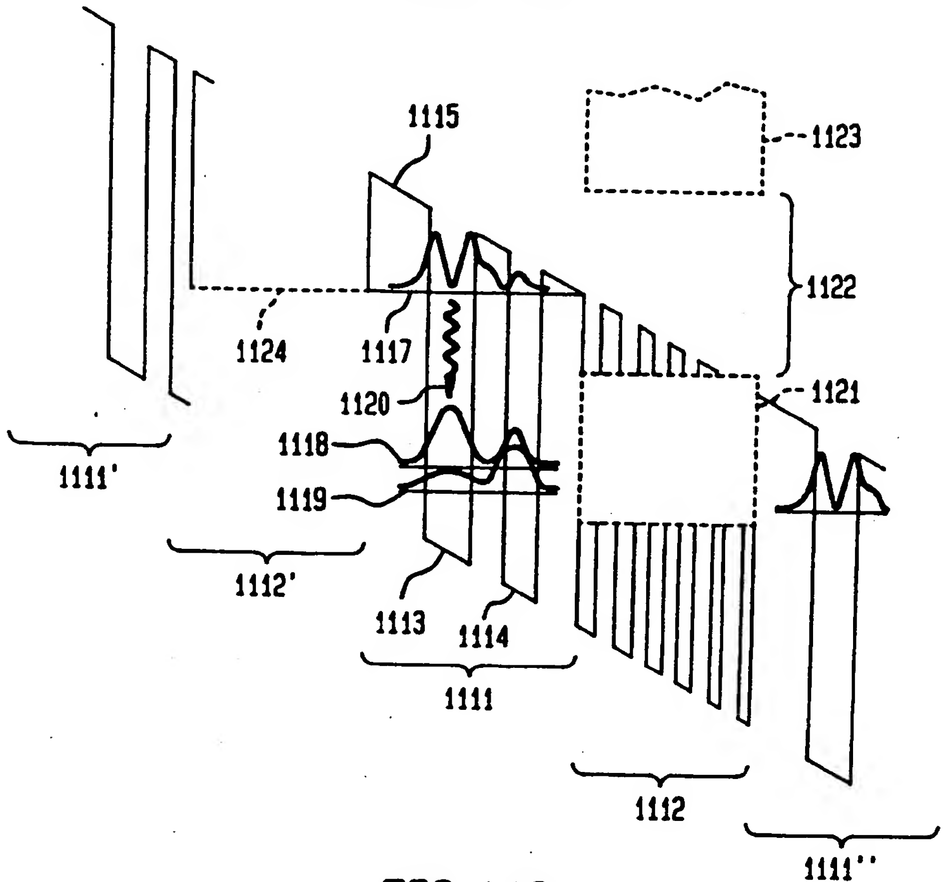
1115
1123
1122
1121
1124
1117
1120
1118
1119
1111'
1112'
1113
1114
1111
1112
1111''

FIG. 12

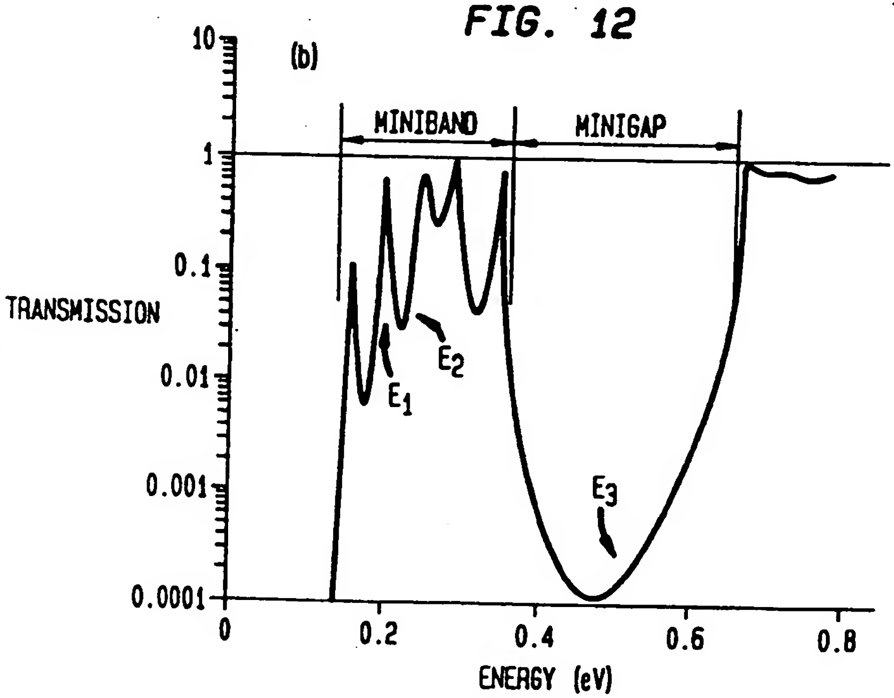
10
1
0.1
0.01
0.001
0.0001
(b)
MINIBAND
MINIGAP
TRANSMISSION
E1
E2
E3
0
0.2
0.4
0.6
0.8
ENERGY (eV)

FIG. 13

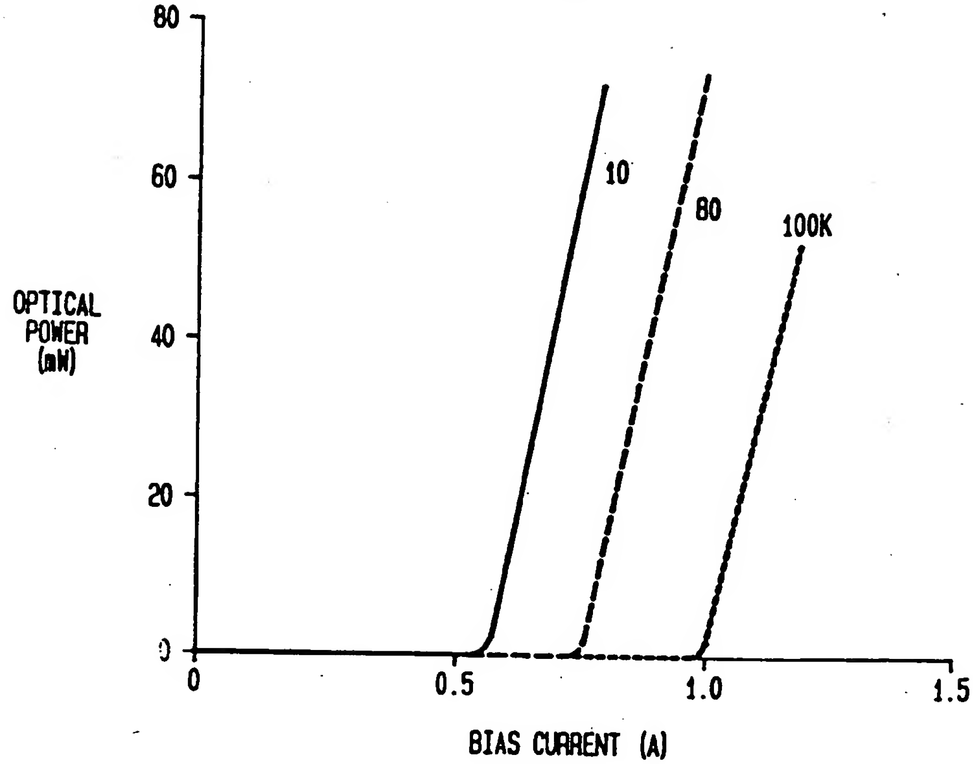
80
60
40
20
0
OPTICAL
POWER
(mW)
10
80
100K
0
0.5
1.0
1.5
BIAS CURRENT (A)

FIG. 14

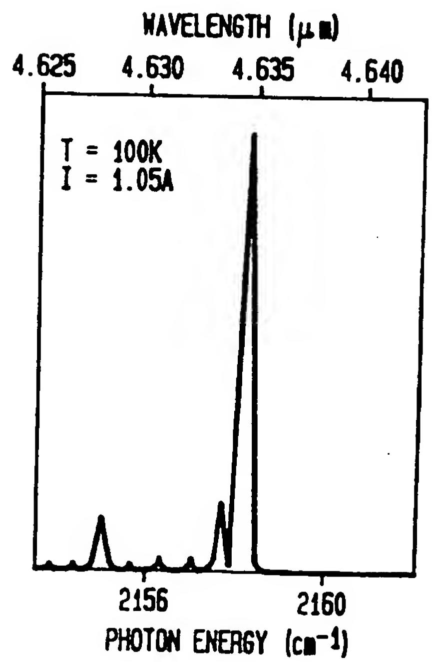
WAVELENGTH (μm)
4.625
4.630
4.635
4.640
T = 100K
I = 1.05A
2156
2160
PHOTON ENERGY (cm-1)

European Patent Office

EUROPEAN SEARCH REPORT

Application Number
EP 95 30 2112

DOCUMENTS CONSIDERED TO BE RELEVANT

Category	Citation of document with indication, where appropriate, of relevant passages	Relevant to claim	CLASSIFICATION OF THE APPLICATION (Int.Cl.6)
D,X	APPLIED PHYSICS LETTERS, vol. 59, no. 21, 18 November 1991 pages 2636-2638, XP 000265170 KASTALSKY A ET AL 'POSSIBILITY OF INFRARED LASER IN A RESONANT TUNNELING STRUCTURE' * the whole document * ---	1-4,7,9	H01S3/18 H01S3/19
D,X	APPLIED PHYSICS LETTERS, vol. 64, no. 9, 28 February 1994 NEW YORK US, pages 1144-1146, XP 000425924 J. FAIST ET AL 'Mid-infrared field tunable intersubband electroluminescence at room temperature by photon assisted tunneling in coupled quantum wells' * the whole document * ---	1-6	
D,A	APPLIED PHYSICS LETTERS, vol. 63, no. 8, 23 August 1993 NEW YORK US, pages 1089-1091, Y.M. YEE ET AL 'carrier transport and intersubband population inversion in coupled quantum wells' * the whole document * ---	1	TECHNICAL FIELDS SEARCHED (Int.Cl.6) H01S
A	US-A-5 128 728 (LIU HUI C) 7 July 1992 * the whole document * ---	1	
A	FR-A-2 607 978 (THOMSON CSF) 10 June 1988 * the whole document * --- -/--	1	

The present search report has been drawn up for all claims

Place of search	Date of completion of the search	Examiner
THE HAGUE	13 July 1995	Claessen, L

CATEGORY OF CITED DOCUMENTS

X : particularly relevant if taken alone
Y : particularly relevant if combined with another document of the same category
A : technological background
O : non-written disclosure
P : intermediate document

T : theory or principle underlying the invention
E : earlier patent document, but published on, or after the filing date
D : document cited in the application
L : document cited for other reasons
& : member of the same patent family, corresponding document

EPO FORM 1503 03.82 (P04C01)

European Patent Office

EUROPEAN SEARCH REPORT

Application Number
EP 95 30 2112

DOCUMENTS CONSIDERED TO BE RELEVANT

Category	Citation of document with indication, where appropriate, of relevant passages	Relevant to claim	CLASSIFICATION OF THE APPLICATION (Int.Cl.6)
P,X	ELECTRONICS LETTERS, vol. 30, no. 111, 29 May 1994 STEVENAGE GB, pages 865-866, XP 000465042 J. FAIST ET AL 'Quantum cascade laser. An intersuband semiconductor laser operating above liquid nitrogen temperature' * the whole document *	1-6,9,10	
P,X	APPLIED PHYSICS LETTERS, vol. 66, no. 5, 30 January 1995 NEW YORK US, pages 538-540, J. FAIST ET AL 'Vertical transition quantum cascade laser with Bragg confined excited state' * the whole document *	1-4,7-10	

TECHNICAL FIELDS SEARCHED (Int.Cl.6)

The present search report has been drawn up for all claims

Place of search	Date of completion of the search	Examiner
THE HAGUE	13 July 1995	Claessen, L

CATEGORY OF CITED DOCUMENTS

X : particularly relevant if taken alone
Y : particularly relevant if combined with another document of the same category
A : technological background
O : non-written disclosure
P : intermediate document

T : theory or principle underlying the invention
E : earlier patent document, but published on, or after the filing date
D : document cited in the application
L : document cited for other reasons

& : member of the same patent family, corresponding document